Nucleic Acids Research, 2025, **53**, gkaf102
https://doi.org/10.1093/nar/gkaf102
Molecular and Structural Biology

Structural basis of endo-siRNA processing by Drosophila Dicer-2 and Loqs-PD

Na Cao[1,†], Jia Wang[1,*,†], Ting Deng[2,†], Boming Fan[2], Shichen Su[2], Jinbiao Ma[2,*], Hong-Wei Wang[1,*]

[1]Ministry of Education Key Laboratory of Protein Sciences, Tsinghua-Peking Joint Center for Life Sciences, Beijing Advanced Innovation Center for Structural Biology, Beijing Frontier Research Center of Biological Structures, State Key Laboratory of Membrane Biology, School of Life Sciences, Tsinghua University, Beijing 100084, China
[2]State Key Laboratory of Genetic Engineering, Collaborative Innovation Centre of Genetics and Development, Department of Biochemistry and Biophysics, Institute of Plant Biology, School of Life Sciences, Fudan University, Shanghai 200438, China

[*]To whom correspondence should be addressed. Email: hongweiwang@tsinghua.edu.cn
Correspondence may also be addressed to Jinbiao Ma. Email: majb@fudan.edu.cn
Correspondence may also be addressed to Jia Wang. Email: wangjia2016@tsinghua.edu.cn
[†]Na Cao, Ting Deng, and Jia Wang contributed equally to this work.

Abstract

Endogenous small interfering RNAs (endo-siRNAs or esiRNAs) originate from either elongated endogenous transcripts capable of forming complex fold-back structures or from double-stranded regions generated through intermolecular base pairing of convergently transcribed mRNAs. The mechanism of maturation and functionality of esiRNAs exhibit significant variation across diverse species. In *Drosophila melanogaster*, esiRNAs reside in both somatic and germline cells, where they serve as post-transcriptional modulators for specific target RNAs. Their maturation process critically relies on Dicer-2 (Dcr-2), with the assistance of its cofactor Loqs-PD. In this study, we have successfully elucidated the cryo-EM structures of Dcr-2/Loqs-PD complex bound to esiRNA precursors (pre-esiRNAs) in various states. Our structural and biochemical results reveal that ATP is essential for the cleavage of esiRNAs by the Dcr-2/Loqs-PD complex, a process analogous to the cleavage of double-stranded RNA (dsRNA). When Loqs-PD is present, pre-esiRNAs are preferentially loaded onto the Helicase domain of Dcr-2. Moreover, as the Helicase domain exhibits a preference for binding to the rigid end of double-stranded RNA, Dcr-2 tends to cleave pre-esiRNA from the small closed loop end, rather than the loose and flexible open end.

Graphical abstract

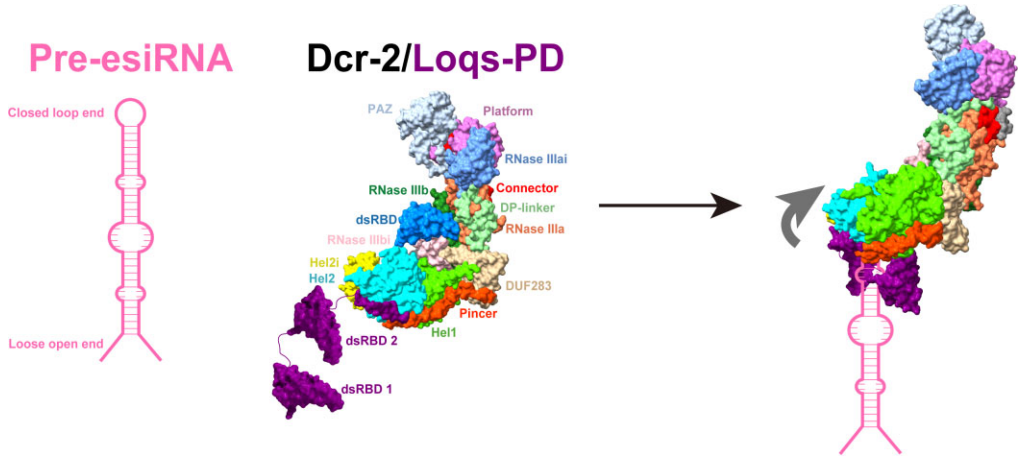

Introduction

RNA interference (RNAi) is a highly conserved mechanism of RNA silencing that plays a pivotal role in regulating gene expression, defending against viral infections, and protecting the genome from transposon activity. This process operates at both the post-transcriptional and epigenetic levels [1, 2]. All RNAi pathways share a common effector complex, which consists of an argonaute protein paired with a short

Received: October 30, 2024. **Revised:** January 21, 2025. **Editorial Decision:** January 31, 2025. **Accepted:** February 5, 2025

single-stranded RNA molecule. These argonaute–RNA complexes possess the capability to repress gene transcription, trigger site-specific cleavage of target messenger RNA (mRNA), or hinder mRNA translation [3, 4]. Based on their biogenesis pathways and the specific argonaute proteins with which they associate, these small RNAs can be classified into three categories: microRNAs (miRNAs), small interfering RNAs (siRNAs), and Piwi-interacting RNAs (piRNAs) [5, 6]. Among them, siRNAs can be further subclassified into two types depending on the source of the RNAs: exogenous siRNAs (exo-siRNAs) and endogenous siRNAs (endo-siRNAs).

In *Drosophila melanogaster*, the classical pathway of small RNA biogenesis involves RNase III proteins and their cofactor proteins, ultimately culminating in the execution of the silencing function with the assistance of argonaute proteins. For instance, miRNAs originate from local hairpin structures through the enzymatic activity of two RNase III proteins: Drosha and Dicer-1 (Dcr-1) [7–10]. These mature miRNAs, typically measuring ∼22 nucleotides in length [11], predominantly associate with the argonaute-1 (Ago-1) [12] to modulate the expression of protein-coding genes. On the other hand, siRNAs are generated by Dicer-2 (Dcr-2), whose Helicase domain possesses a DExDc region capable of ATP binding, a feature absent in Dcr-1 [13]. They normally consist of 21 nucleotides and associate with argonaute-2 (Ago-2) to assemble the RNA-induced silencing complex (RISC) [14]. Despite the fact that the domains as well as their spatial arrangements of Dcr-1 and Dcr-2 are highly similar, there are significant differences in the processes for their respective substrates. The 5′- and 3′-ends of the miRNA precursors first bind to the Platform and Piwi/Argonaute/Zwille (PAZ) domains of Dcr-1; in contrast, the precursors of siRNA first bind and translocate the Helicase domain of Dcr-2 before reaching the Platform/PAZ domains. The RNase III proteins involved in the above processes are typically modulated or facilitated by their cofactor proteins, which are mostly double-stranded RNA-binding proteins (dsRBPs) [15–17]. These dsRBPs generally consist of multiple double-stranded RNA-binding domains (dsRBDs) connected by linkers of varying length. Drosha's partner protein, Pasha, possesses two dsRBDs [18], while Dcr-1 and Dcr-2 rely on various isoforms of the Loqs family of proteins [19, 20]. Alternative splicing of Loqs transcripts results in the generation of four distinct isoforms: Loqs-PA, PB, PC, and PD [20, 21]. Among them, Loqs-PA and Loqs-PB, which are homologs of the human Dicer cofactor TRBP, interact with Dcr-1 during the biogenesis of miRNA [22]. Loqs-PC is rarely expressed and its function remains unknown, whereas Loqs-PD is crucial in Dcr-2-dependent endo-siRNA biogenesis [23, 24].

Endo-siRNAs (abbreviated as esiRNAs) represent a novel class of small RNAs in RNAi pathway and have been identified in both somatic and germline cells [25, 26]. Compared to miRNA, exo-siRNA, and piRNA, research on the functions of esiRNAs is rather limited. The esiRNAs were first discovered in *Caenorhabditis elegans* [27, 28] and subsequently in other species, with their functions demonstrating substantial disparities [29]. In fission yeast, esiRNAs, which are produced from repetitive sequences in chromosome pericentromeres, are also found there, where they are involved in the formation of heterochromatin and transcriptional gene silencing [30, 31]. In mice, esiRNAs are rarely detected in somatic cells, but they are prevalent in ovaries and early pre-implantation embryos [32, 33]. The biogenesis and function of esiRNAs have unique characteristics when compared to those of miRNAs and siRNAs. Specifically, in oocytes, esiRNAs are generated by a distinct Dicer isoform, which targets maternal mRNAs and performs diverse functions in the regulation of gene expression [34]. In humans, esiRNAs originate from antisense transcription of the PPM1K gene, either directly forming structured RNA or creating double-stranded RNAs with their corresponding mRNA [35].

In *Drosophila*, esiRNAs are produced from the processing of their precursors by Dcr-2, rather than Drosha and Dcr-1. These 21-nucleotide esiRNAs originate from a diverse array of endogenous double-stranded RNA sources, including transposons (TEs), *cis*-natural antisense transcripts (*cis*-NATs), *trans*-NATs, and hairpin RNA transcripts (hpRNAs) [36]. These esiRNAs function in regulating gene expression, silencing transposons, and facilitating heterochromatin formation, thereby attaining their gene silencing effects [37]. In *Drosophila*, the precursors of esiRNAs predominantly originate from two distinct gene loci. One locus, CG18854, generates a structured double-stranded RNA of ∼400 base pairs, referred to as esi-1. The other locus, CG4068, comprises a sequence of 20 palindromic repeats, each spanning ∼260 nucleotides and forming hairpin structures, labeled as esi-2 [38, 39]. Despite the identification of esiRNAs, their biological and molecular mechanisms remain poorly understood.

Although our previous studies have shown that Dcr-2 undergoes conformational changes during the translocation, dicing, and post-dicing states of dsRNA processing, mediated by ATP hydrolysis [40], unfortunately, we were unable to obtain the structure of the pre-dicing state. Moreover, the resolution of the structures of the initial binding and dicing states is insufficient, preventing us from gaining deeper insights into the interactions between Dcr-2 and/or Loqs-PD and their RNA substrates. To elucidate the molecular mechanism of esiRNA biogenesis, particularly during Dcr-2 processing, we have solved several high-resolution cryo-EM structures of Dcr-2/Loqs-PD complexed with esiRNA precursors, capturing the initial binding, pre-dicing, and dicing states. Analysis of these structures revealed additional details regarding the interactions between Dcr-2/Loqs-PD and RNA. During the processing of esiRNA, Loqs-PD exhibits the capability to modulate Dcr-2's initial binding location of esiRNA precursors. Additionally, we conducted an examination to determine of Dcr-2's primary cleavage site on the esiRNA precursor.

Materials and methods

Protein expression and purification

Plasmid construction and protein purification were prepared as described previously [40]. Dcr-2 or its mutation (Dcr-2^{DDNN}) was constructed onto pFastBac plasmid. Loqs-PD and its mutations were cloned to modified pET28a. Dcr-2 was transfered in sf9 cells by using Bac-to-Bac baculovirus expression system. Cells expressing the target protein were harvested and then purified by Ni-NTA affinity, Hitrap Q column (Cytiva), and a Superdex 200 10/300 Increase column (Cytiva). Loqs-PD was purified from *Escherichia coli* by 6 × His tag. Then, 6 × His tag was removed via cleavage by TEV protease overnight, and the protein solution was run again through Ni-NTA affinity chromatography before further purification through Superdex 200 10/300 Increase column (Cytiva).

RNA transcription and purification

The pre-esiRNAs were prepared by *in vitro* transcription using HiScribe® T7 High Yield RNA Synthesis Kit (NEB, E2040S). RNA transcription carried out according to the kit instructions. Then, GIP (NEB, M0525) and T4 PNK (NEB, M0201) are successively added to generate the 5′-phosphate and remove the 2′,3′-cyclic phosphate at the 3′-end of the RNA. Subsequently, phenol–chloroform method was used for RNA precipitation, and it was resuspended in Ultrapure water without RNase enzyme. In the end, RNA was purified by size-exclusion chromatography using the Superdex 200 3.2/300 Increase column (Cytiva). The RNA sequences are listed in Supplementary Table S2.

In vitro dsRNA cleavage assays

Cleavage assays of Dcr-2 or its complex (0.6 μM) with dsRNA substrate (0.9 μM) were performed in cleavage buffer (50 mM Tris, pH 8.0, 150 mM NaCl, 5 mM ATP, and 5 mM $MgCl_2$) with dsRNA. The reactions were stopped with equal volume of 2 × formamide loading buffer. Samples were separated by 12% denaturing PAGE and stained with GelRed. ImageJ was used for data analysis. Three independent trials were conducted.

Cryo-EM sample preparation and data collection

The Dcr-2^{DDNN}/Loqs-PD was mixed with slm1 or slm2, followed by the addition of 5 mM ATP and $MgCl_2$, and then incubated at room temperature for 3 h. In meanwhile, protein complexes incubated with slm2 without ATP and Mg^{2+} for initial binding structure analysis. Using an FEI Vitrobot MarkIV at 8°C and 100% humidity, 4 μl of specimen was loaded onto a reduced graphene oxide grid (Quantifoil Au 1.2/1.3, 300 mesh) [41], which had been pretreated with glow discharge for 10 s at a middle level after a 2-min evacuation, and then blotted with a filter paper for 0.5 s after a 1-min incubation. The grid was immediately vitrified by plunging into pre-cooled liquid ethane. Cryo-EM data were collected on different 300 kV Titan Krios electron microscopes equipped with Gatan K3 direct electron detector and Gatan Quantum energy filter. All data were automatically recorded using AutoEMation [42] or EPU in counting mode and defocus values ranged from −1.5 to −2.0 μm.

Image processing and 3D reconstruction

The raw dose-fractionated image stacks were processed using MotionCorr2 [43] for two times Fourier binning, alignment, dose-weighting, and summation. In CryoSPARC [44], the contrast transfer function (CTF) parameters were estimated using Patch-CTF or CTFFIND4 [45]. A large number of initial particles were automatically picked from high-quality micrographs that filtered out by blob picker. High-quality particles were screened after several rounds of reference-free 2D classification and then transferred into Relion for several rounds of 3D classification. Particles from better 3D classes were processed by high-resolution homogeneous refinement in CryoSPARC.

Model building and refinement

The previously determined cryo-EM structure of Dcr-2 (PDB: 7W0E) was docked into the high-resolution EM density map by ChimeraX [46] and used as the initial models, and then adjusted manually by ISOLDE in ChimeraX and COOT [47]. Finally, all the models were refined against the EM map by PHENIX [48] in real space with secondary structure and geometry restraints. The final models were validated in PHENIX software package. The model statistics are summarized in Supplementary Table S1.

Results

Structural determination and structural details

In order to investigate the biochemical and structural mechanism of esiRNA processing by Dcr-2, we set up an *in vitro* system with recombinant proteins and RNA precursors (Fig. 1). We reconstituted the full-length Dcr-2/Loqs-PD complex by incubating Dcr-2 purified from insect SF9 cells with Loqs-PD purified from *E. coli* ("Materials and methods" section and Supplementary Fig. S1). For esiRNA precursors, we selected the two most frequently reported genes of endo-siRNA precursors in *Drosophila* somatic cells, esi-1 and esi-2, and predicted the secondary structure of their transcriptional products (Supplementary Fig. S2). In contrast to pre-miRNA, a single esiRNA precursor can be processed to generate multiple mature esiRNAs with distinct functionalities. To facilitate biochemical and structural analysis, we truncated 96 nucleotides from the middle region of esi-1 and introduced point mutations, thus generating a representative esi-1 precursor (named as slm1). This region of slm1 was demonstrated to produce multiple abundant esiRNAs that exhibit significant complementarity to the protein-coding gene CG8289 [38]. We also truncated 104 nucleotides from one end of esi-2 to generate a representative esi-2 precursor (named as slm2), from which numerous consecutive and phased esiRNA duplexes were cloned [24, 39]. In our design, both slm1 and slm2 adopt hairpin structures, with one end containing a 5′-monophosphate and a 2-nt 3′-overhang, and the other end featuring a small loop (Supplementary Fig. S2). *In vitro* cleavage assays showed that both slm1 and slm2 can be effectively processed by the reconstituted Dcr-2/Loqs-PD complex in the presence of magnesium and ATP (Supplementary Fig. S3). Significantly, Dcr-2/Loqs-PD exhibited a markedly enhanced cleavage efficiency for slm1, whereas the cleavage level for slm2 was comparatively lower. We speculate that this discrepancy is likely attributable to the higher frequency of mismatched bases present in the slm2 sequence, which may affect the translocation activity of Helicase domain. Furthermore, Dcr-2/Loqs-PD also generated a variety of noncanonical cleavage products when processing slm2, predominantly characterized by products of ∼30 and 42 nt (blue arrows) in length (Supplementary Fig. S3B).

To elucidate the structural mechanism of esiRNA-processing activity by the Dcr-2/Loqs-PD complex, the dicing-deficient mutant Dcr-2/Loqs-PD complex, as described previously [40], was incubated with slm1 or slm2 in a reaction buffer containing magnesium ions and ATP for ∼3 h prior to cryo-EM structural analysis. We obtained cryo-EM structures of the Dcr-2/Loqs-PD complex bound to slm1 and slm2 at 4.1 and 3.5 Å resolutions, respectively (Fig. 1B and D, and Supplementary Fig. S4). The structures revealed that Dcr-2/Loqs-PD complex can form stable complexes with both RNAs but at different states of the dicing process (Fig. 1C and E). In comparison with previous structures of Dcr-2 processing dsRNA [40], the structure of Dcr-2 with

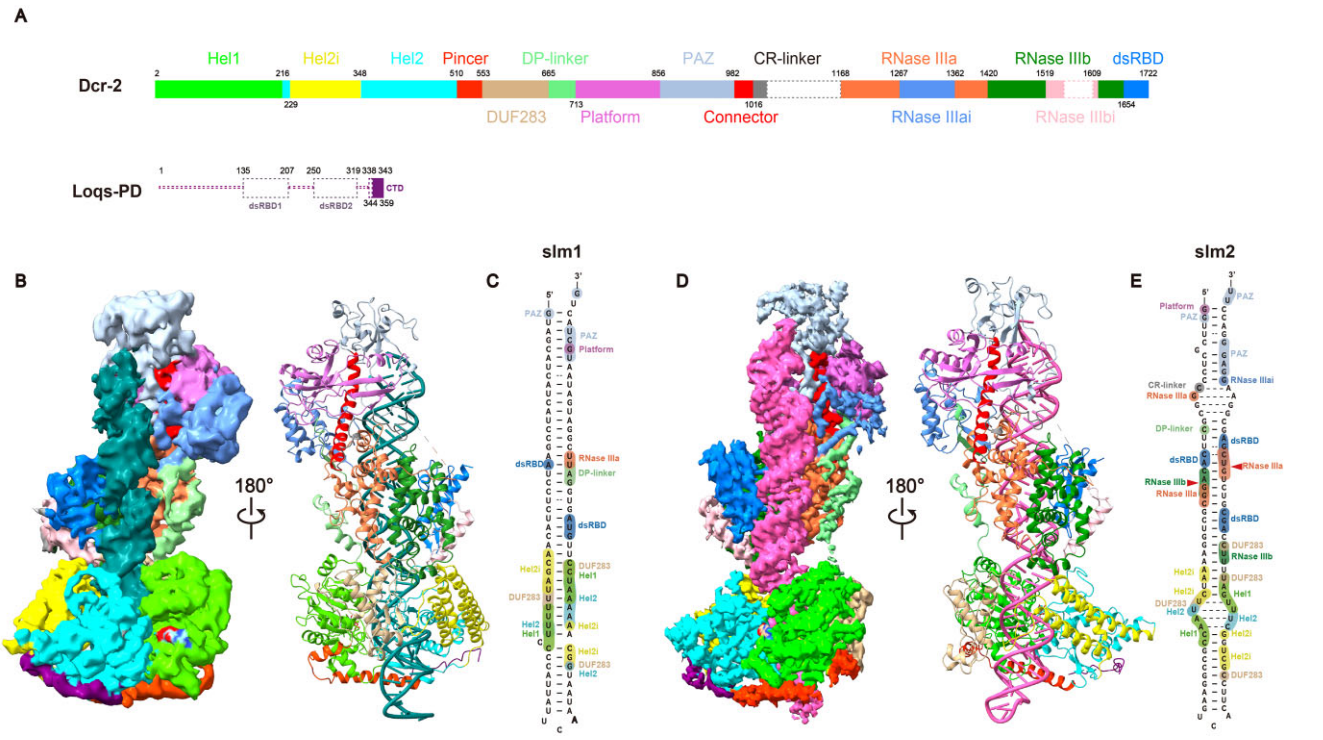

Figure 1. Cryo-EM structures of the Dcr-2/Loqs-PD complex in the dicing and pre-dicing states with pre-esiRNAs. (**A**) Schematic illustration of the domain arrangement of Dcr-2 and Loqs-PD. Disordered segments are represented by dashed lines. (**B**) Overall cryo-EM density map and cartoon model of Dcr-2/Loqs-PD/slm1 in the pre-dicing state. (**C**) Schematic diagram showing the interactions between the Dcr-2 and slm1 in the pre-dicing state. The bases involved in Watson–Crick base pairing are connected with a solid line, whereas the rest are placed separately or connected through dashed lines [same for (E)]. (**D**) Overall cryo-EM density map and cartoon model of Dcr-2/Loqs-PD/slm2 in the dicing state. The display mode is the same as in panel (B). The color of slm2 is pink. (**E**) Schematic diagram showing the interactions between the Dcr-2 and slm2 in the active dicing state. Red arrows indicate dicing sites. Unless specified otherwise, the color scheme of Dcr-2, Loqs-PD, slm1, and slm2 is used throughout all of the figures.

slm1 represents a novel state that has not been observed previously, which we term as the "pre-dicing state" based on its structural feature. Conversely, the structure of the complex formed by Dcr-2 with slm2 depicts an active dicing state of esiRNA precursor.

The structure of Dcr-2 with slm2 revealed more detailed interactions between the protein and RNA substrate in the dicing state than the previous structures, owing to its higher resolution (Supplementary Figs S5, S11B and C). Analogous to Dicer homologs, the 5′-monophosphate and 3′-overhang termini of slm2 are stably anchored within the 5′ and 3′ pockets formed by the Platform/PAZ domains through hydrogen bonds. The monophosphate of guanosine nucleotide (G1) located at the 5′ terminus of slm2 inserts into the 5′ pocket, forming hydrogen bonds with Asn773 and Tyr740 residues within the Platform domain (Supplementary Fig. S5A). Within the 3′ pocket, two conserved tyrosine residues, Tyr886 and Tyr925, situated in the PAZ domain, establish robust interactions via hydrogen bonding with the phosphodiester bond of the uridine nucleotide (U104) positioned at the 3′ terminus (Fig. 3B and Supplementary Fig. S5B). Upon comparing the sequences of the Platform/PAZ domains of various Dicer proteins, it was discovered that the 3′ binding pocket exhibits higher conservation than the 5′ binding pocket, which is mediated by highly conserved tyrosine residues (Supplementary Fig. S6). In the pre-dicing state structure, although one end of slm1 has reached the Platform/PAZ domains, the configuration differs from the dicing state, as the 3′ terminus of slm1 does not stably bind to the PAZ domain (Fig. 3A). The specific implications of this will be discussed in the later sections.

In proximity to the dicing sites, slm2 is sandwiched between the two RNase III domains and the C-terminal dsRBD. The nucleic acid backbone experiences noticeable conformational changes as it is drawn toward the catalytic active center, indicative of a state poised for cleavage (Supplementary Fig. S5C and D). Consistent with other previously reported RNase III family structures, the double-stranded stem regions of slm2 are respectively attached to RNase IIIa and RNase IIIb domains, enabling the cleavage position to be unequivocally identified at this resolution. The active sites of classical RNase III domain are predominantly constituted by four acidic amino acids that bind to Mg^{2+} ions to exert the cleavage activity [49]. In the cryo-EM map of the dicing state structure of slm2, apart from amino acids and RNA, there is discernible additional density, presumably attributable to Mg^{2+} ions. Based on previous structures, we place the Mg^{2+} ions in the corresponding sites [40]. RNase IIIb and RNase IIIa exhibit dicing activity on scissile phosphodiester bonds, coinciding with the actual cleavage sites between A22 and G23 in the 5′ terminus strand and between G83 and U84 in the 3′ terminus strand, respectively (Supplementary Fig. S5C and D). In the pre-dicing state, slm1 also binds to the dsRBD. However, compared to the dicing state, the conformation and position of the dsRBD do not change significantly, and slm1 is positioned ∼10 Å away from the dicing site, thereby avoiding of dicing by RNase III domains (Supplementary Fig. S7A).

Conformational changes of Dcr-2 during the whole process of substrate dicing

With the solved structure of Dcr-2's pre-dicing state, we now have obtained the whole spectra of Dcr-2's structural states during its processing of RNA substrates. Based on previous findings, Dcr-2 undergoes continuous conformational changes throughout the substrate's dicing process. The newly obtained pre-dicing and high-resolution dicing state structures have significantly enhanced our understanding of Dcr-2's functional attributes. A comparison of the structures of Dcr-2 in the mid-translocation state (PDB: 7W0E) and the pre-dicing state reveals that the overall conformation of Dcr-2 remains consistent during the substrate translocation process (Fig. 2A and B). This also suggests that there is no significant conformational change in Dcr-2 during the initial RNA-binding through its N-terminal Helicase domain up to the pre-dicing state. Therefore, during the upward translocation of RNA, the stable conformation of Dcr-2 ensures the unobstructed passage of the RNA substrate, precluding the imposition of steric hindrance along its path. Structural comparison of Dcr-2 in the pre-dicing state and the dicing state reveals no displacement in the cap and dicing parts, while the Helicase/DUF283 domains exhibit obvious positional changes (Fig. 2C and D). Specifically, the Helicase domain undergoes a rotation of ∼40° around the DUF283 domain (Fig. 2E), although the overall structure of each domain remains unchanged (Supplementary Fig. S8). Higher resolution reveals detailed information regarding the structural changes. The α1 helix of the DP-linker, which links between the DUF283 and Platform domains, transitions from a bent conformation to an elongated state and part of the α1 stretches to form a loop. The relative distance between the α1 of the DP-linker and the α2 of DUF283 increases, ultimately leading to the dissociation of DUF283 from RNase IIIb and alleviating the spatial hindrance for RNA access to the dicing site (Fig. 2F and G). This conformational change is of critical importance for the transition from the pre-dicing state to the dicing state.

Conformational remodeling of the RNA substrates by Dcr-2 during dicing process

The dicing process of Dcr-2 with substrates is also accompanied by conformational changes in the substrate RNAs, particularly notable changes in the binding mode and binding sites on Dcr-2. Although there is no significant conformational change in Dcr-2 from the initial binding to the pre-dicing states, the overall structure of the RNA undergoes substantial alterations during translocation through the Helicase domain driven by ATP hydrolysis. In comparison to the mid-translocation state, ∼12 more bp of duplex thread through the Helicase domain toward the PAZ domain in the pre-dicing state. A closer examination of the structure of Dcr-2 in complex with slm1 in the pre-dicing state suggests that, although the 3′ terminus of slm1 reaches the PAZ domain of Dcr-2, the domain's 3′ binding pocket remains empty (Fig. 3A and B). Consequently, in the pre-dicing state, slm1 is not yet stably bound to the PAZ domain, and the 5′ terminus has not yet reached the Platform domain (Supplementary Fig. S7B). The trajectory of the substrate RNA in the pre-dicing state is identical to that in the early- and mid-translocation states (Fig. 3C), facilitating the completion of the dsRNA-processing cycle.

Subsequently, ATP hydrolysis propels the RNA further upward, ensuring its stable engagement within the binding pocket of the Platform/PAZ domain. In the dicing state, the 3′ terminus moves one additional nucleotide up and stretches into the 3′ conserved binding pockets (Fig. 3A and B). As three additional bps are translocated through the Helicase domain toward the Platform/PAZ domains, the length of the double-stranded region of RNA above the Helicase domain extends ∼15 Å (Fig. 3D), therefore inducing conformational changes of Dcr-2, particularly the DP-linker (Fig. 2F and G). Concurrently, the conformational alteration of Dcr-2 facilitates the alignment of the substrate RNA with the catalytic active center, thereby initiating the cleavage process (Fig. 3E).

Similar to AtDCL3 and human Dicer, the conformation of dsRNA in the dicing state is significantly different from that of a classical type-A dsRNA [50, 51]. Despite the fact that previously reported structure of Dcr-2 bound to 50-bp dsRNA in the dicing state is not of sufficient resolution to distinguish individual bases [40], a comparison of the RNA backbones between the structure of slm2 with the 50-bp dsRNA in the dicing state can still be performed. The comparison revealed that the conformations of RNAs with different sequences are nearly identical (Fig. 3F). In contrast, when the structure of a type-A dsRNA was overlaid with that of slm2 and the dsRNA in the aforementioned conformations, only the first 10-bp region of dsRNA region aligned well to bind the Platform/PAZ domains, whereas the RNA backbone surrounding the cleavage site exhibited a significant deviation (Fig. 3G). This suggests that Dcr-2 enforces a specific conformational change on the substrate RNA in the dicing state, independent of its sequence, to ensure efficient cleavage of the substrate and precise control over the length of the cleavage products (Supplementary Video S1).

Loqs-PD's role in mediating RNA substrates to Dcr-2

In the cryo-EM maps of the Dcr-2/Loqs-PD complex with slm1 or slm2 presented above, the density of most of the Loqs-PD region remains unsolved, except for its C-terminal tail that binds to the Helicase domain of Dcr-2. This is in sharp contrast to the structure of Dcr-1/Loqs-PB with pre-miRNA, in which the Lops-PB binds to pre-miRNA near the dicing site [52]. This implies that, unlike Loqs-PB, Loqs-PD may not directly affect the cleavage process of RNA substrates by RNase domains of Dcr-2. This implication is supported by the high similarity between structures of Dcr-2 in the dicing state on dsRNA and slm2 substrates. Thus, we speculate that the primary function of Loqs-PD in dsRNA or endo-siRNA processing resides in modulating the recruitment of substrates by Dcr-2. To verify this hypothesis, we deemed to investigate the initial substrate recruitment state of Dcr-2 in the presence and absence of Loqs-PD. To achieve this, we separately performed cryo-EM structural analysis of Dcr-2/Loqs-PD in complex with slm2 and Dcr-2 alone in complex with slm2, both in the absence of ATP (Supplementary Fig. S9).

The structure of the Dcr-2/Loqs-PD complex with slm2, obtained in the absence of ATP at a resolution of 3.2 Å, exhibits a similar dimeric arrangement to the initial binding state of dsRNA as determined previously (Fig. 4A) [40]. The C-terminal tail of Loqs-PD wraps over the surface of the Hel2i domain, which interacts with another Dcr-2 to form a dimer (Supplementary Fig. S9A). Interestingly, the

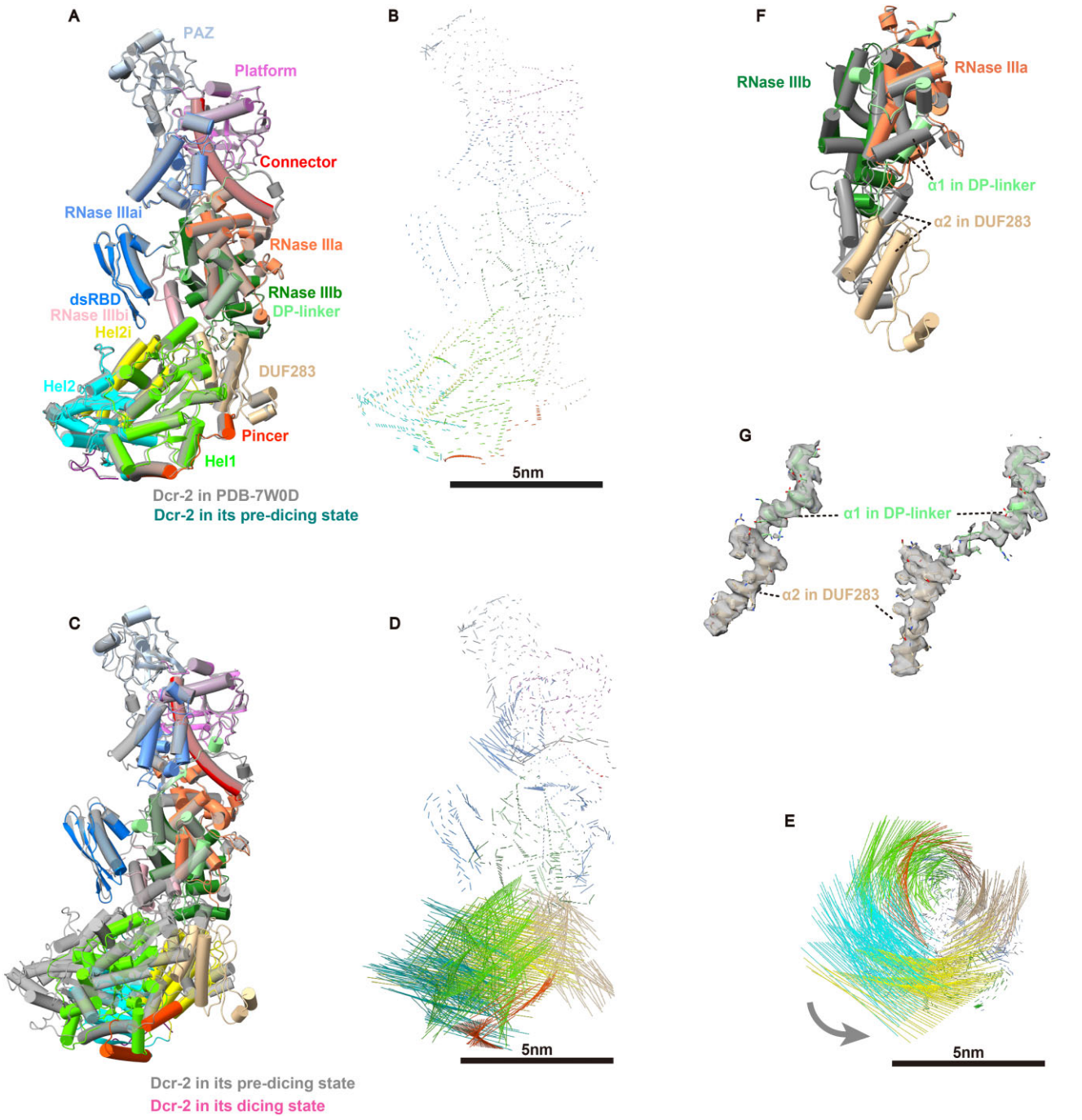

Figure 2. Structural comparison of Dcr-2 in the mid-translocation, pre-dicing, and active dicing states. (**A**) Structural comparison between the pre-dicing state of Dcr-2 in Dcr-2/Loqs-PD/slm1 complex and the mid-translocation state of Dcr-2 in Dcr-2/Loqs-PD/50 bp dsRNA complex (PDB: 7W0D) (gray). Models are superimposed on the PAZ and Platform domains [same for (**C**)]. (**B**) Displacement vectors of Dcr-2's Cα coordinates comparison between two states shown in (A). The length of the stick correlates with its displacement. Scale bar: 5 nm [same for panels (**D**) and (**E**)]. (C) Structural comparison between the pre-dicing state of Dcr-2 in Dcr-2/Loqs-PD/slm1 complex (gray) and the active dicing state of Dcr-2 in Dcr-2/Loqs-PD/slm2 complex. (D and E) Displacement vectors of the Dcr-2's Cα coordinates comparison between two states shown in panel (C). (E) Displacement vectors shown from the bottom view of panel (D). The direction of movement is marked by the gray arrow. (**F**) Structural comparison between the pre-dicing state of Dcr-2's DP-linker and DUF283 domains in Dcr-2/Loqs-PD/slm1 complex (gray) and these domains of Dcr-2/Loqs-PD/slm2 complex in the active dicing state. Models are superimposed on the RIIIDa and RIIIDb domains. (**G**) Cryo-EM density maps and cartoon models of α1 helix in the DP-linker and α2 helix in the DUF283 domain in the pre-dicing (left) and active dicing (right) states, respectively.

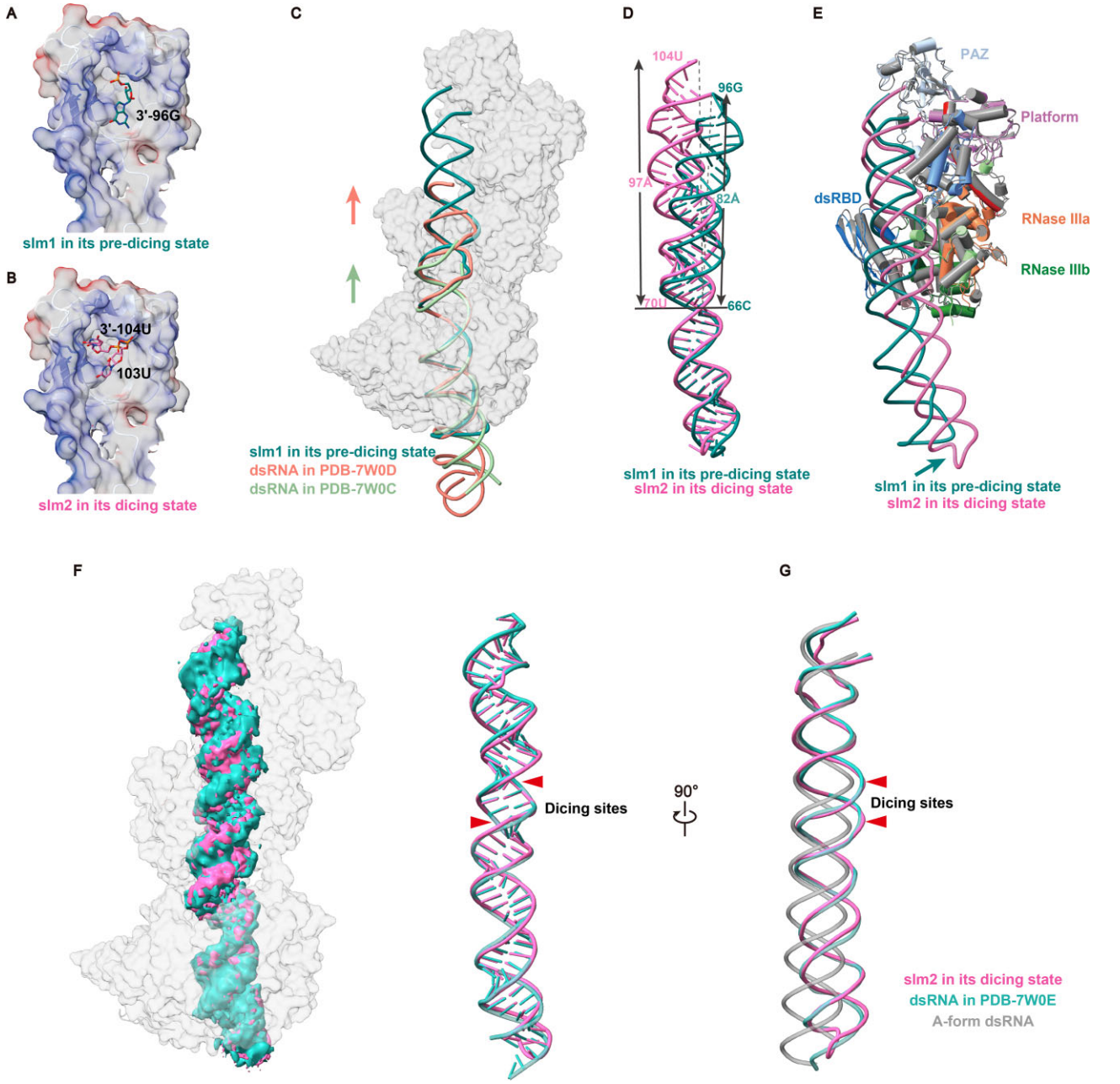

Figure 3. Structural comparison of dsRNA in the early- and mid-translocation, pre-dicing and active dicing states. (**A** and **B**) The 3′-terminus of slm1 (A) or slm2 (B) during different positional relationships with the PAZ domain. The electrostatic potential surface of the PAZ domain is shown in transparent. (**C**) Superimposition of the Dcr-2/Loqs-PD/slm1 in the pre-dicing state, the Dcr-2/Loqs-PD/50 bp dsRNA in the early- (PDB: 7W0C) and mid-translocation (PDB: 7W0D) states by the Dcr-2 protein. The Dcr-2 in the pre-dicing state is shown with a transparent surface [same for (F)]. The direction of movement is marked by arrows. (**D**) Superimposition of slm1 in the pre-dicing state and slm2 in the active dicing state by Helicase domain. (**E**) Superimposition of the Dcr-2/Loqs-PD/slm1 in the pre-dicing state and the Dcr-2/Loqs-PD/slm2 in the active dicing state. Models are superimposed on the PAZ and Platform domains. The direction of movement is marked by arrow. (**F**) Superimposition of the Dcr-2/Loqs-PD/50 bp dsRNA (PDB: 7W0E) and the Dcr-2/Loqs-PD/slm2 in the dicing state. The cryo-EM density maps and the cartoon models are shown in the left and right, respectively. The arrows indicate dicing sites [same for (**G**)]. (G) Superimposition of slm2, 50 bp dsRNA (PDB: 7W0E) and A-form dsRNA. This view only shows the back-bone trajectory and is rotated 90° relative to panel (F) around the longitudinal direction.

dimerization phenomenon was not observed in the absence of Loqs-PD (Supplementary Figs S9E and S10), suggesting that Loqs-PD plays a crucial role in the dimerization process of Dcr-2. In this structural state, the slm2 is wrapped around by the Helicase domain and bound by one dsRBD of Loqs-PD in a classic three-point binding manner (Fig. 4B and C) [53]. However, due to its flexibility, another dsRBD of Loqs-PD was not observed in this structure.

In contrast, the cryo-EM structure of Dcr-2 in complex with slm2, obtained in the absence of ATP at resolution of 6.2 Å, revealed a monomeric Dcr-2 bound to single slm2 molecule. In this structural state, we can clearly observe one end of slm2 binding to the Platform-PAZ domains, while the other end passes through the Helicase domain (Fig. 4D and Supplementary Fig. S11A). Since ATP is absent, slm2 is unlikely to be translocated through the Helicase domain. It

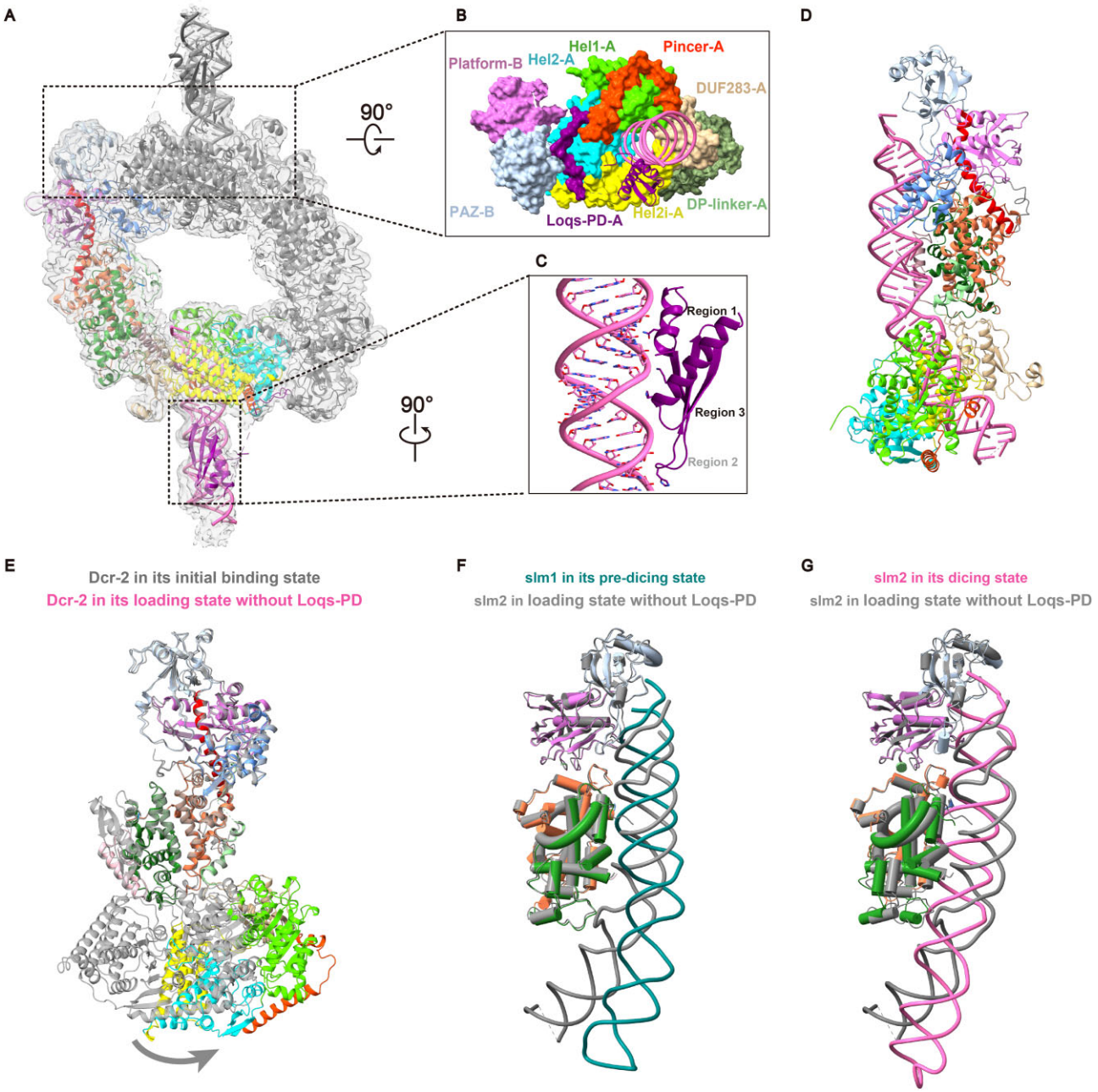

Figure 4. The function of Loqs-PD in pre-esiRNA processing by Dcr-2. (**A**) Overall cryo-EM density map and cartoon model of the Dcr-2/Loqs-PD/slm2 complex in the initial binding state. (**B**) Magnified view of panel (A) from the top view. (**C**) Magnified view of the dsRBD2 domain of Loqs-PD interacting with slm2. (**D**) Cartoon model of Dcr-2–slm2 in the loading state without Loqs-PD. (**E**) Structural comparison between the initial binding state of Dcr-2 in Dcr-2/Loqs-PD/slm2 complex (gray) and the loading state of Dcr-2 in the Dcr-2–slm2 complex. Models are superimposed on the PAZ and Platform domains. (**F** and **G**) Superimposition of the Dcr-2/Loqs-PD/slm1 complex in the pre-dicing state (F) or the Dcr-2/Loqs-PD/slm2 complex in the dicing state (G) with the Dcr-2–slm2 complex in the loading state, respectively. Models are superimposed on the PAZ and Platform domains. The domains of Dcr-2 in the loading state are colored in gray.

is probably loaded directly onto Dcr-2, with one end binding to Platform/PAZ domains and the middle of double-stranded stem being latched by the Helicase domain. This state termed as "loading state" here, due to its distinct conformation compared to all previously captured structures. In this loading state, the DUF283 domain remains attached to RNase IIIb but exhibits a more pronounced angular shift relative to RNase IIIb compared to the initial binding state (Fig. 4E and Supplementary Fig. S11B). The RNA substrate's trajectory is unique and differs from that observed in the pre-dicing and dicing states. Although it follows a path similar to the pre-dicing state near the cap and core modules, it does not approach the cleavage active center but is instead locked by the Helicase domain, with its axis exhibiting an ∼18° bend (Fig. 4F and G). The distance between the RNA and the RNase III catalytic sites during the loading state is ∼12.3 Å, which is greater than the distances of 7.9 and 4.1 Å observed in the pre-dicing and dicing states, respectively. We speculate that in the absence of Loqs-PD, even though slm2 can bind to Dcr-2, the loading state may not represent the correct bind-

ing mode, as Dcr-2 alone shows minimal cleavage activity on slm2, regardless of ATP presence (Supplementary Fig. S11C). Therefore, for slm2, Dcr-2, although capable of binding one end of the substrate like human Dicer through the PAZ domain, is unable to cleave it, with the Helicase domain potentially playing a crucial inhibitory role. The loading state observed *in vitro* is likely due to the unique structure of slm2, which features a 2-nt overhang at its 3′ terminus. In contrast, natural esiRNA precursors, which lack this feature, find it difficult to bind directly to the PAZ domain. Consequently, slm2 must bind to the Helicase domain via Loqs-PD. Only after the Helicase domain hydrolyzes ATP and allows slm2 to pass through can it be efficiently cleaved. In the absence of Loqs-PD, the faint cleavage products may arise from a small amount of slm2 correctly binding to the Helicase domain (Supplementary Fig. S11C). Therefore, for esiRNA precursor substrates, we infer that Loqs-PD primarily functions as an intermediary, facilitating the recruitment and translocation of double-stranded RNA segments to the Helicase domain, thereby ensuring the highly efficient dicing of RNA.

The interaction between dsRBD domains and RNA substrates

In the initial binding state, the dsRBD of Loqs-PD engages with slm2 through three distinct regions. Region 1 and region 2 bind to the minor groove of the dsRNA, whereas region 3 interacts with the major groove. Notably, the interactions between regions 1 and 2 with the dsRNA are robust, involving specific interactions with the 2′-hydroxyl groups of the sugar rings. Conversely, region 3 forms interactions with the non-bridging oxygen atoms of the phosphate backbone (Fig. 4C and Supplementary Fig. S12A). In addition to the dsRBD of the Dcr-2 C-terminal, the DUF283 domain also exhibits dsRBD characteristics. In the dicing state structure, both the C-terminal dsRBD and the DUF283 domain of Dcr-2 adopt the canonical $\alpha\beta\beta\beta\alpha$ topology of a dsRBD and interact with slm2. Nevertheless, they deviate from the conventional three-point binding mechanism observed in dsRBDs with dsRNA, as they possess solely two binding sites with slm2 (Supplementary Fig. S12B and C). Alignment of amino acid sequences among dsRBDs shows that region 2 contains a specific and evolutionarily conserved G**H motif [54], which is absent in both the C-terminal dsRBD and DUF283 domains of Dcr-2 (Supplementary Fig. S12D). Region 2 of the C-terminal dsRBD domain is shorter, whereas the corresponding region in DUF283 is longer and folds into a small α-helix and flips out. The two additional binding sites, binding patterns, and critical amino acids involved in the interactions between the C-terminal dsRBD, DUF283, and dsRNA exhibit a high degree of evolutionary conservation (Supplementary Fig. S12A and D). Region 1 and region 2 interact with the minor groove of dsRNA, and such interaction exhibits a preference for the RNA sequence. Given that region 2 of DUF283 and dsRBD ceases to bind to RNA, their preference for the RNA sequence may be diminished.

End selection of pre-esiRNA by Dcr-2/loqs-PD

Precursors of esiRNA transcribed from genomic structured loci fold into extensive double-stranded RNA stem-loop structures, typically presenting specific ends with a closed small loop at one end and a loose open structure at the other end (Supplementary Fig. S2). Since the mechanisms underlying the processing of esiRNA precursors and dsRNAs by Dcr-2 are similar, both involving ATP hydrolysis to translocate the bound substrate RNAs for complete cleavage, the initial dicing site selected by Dcr-2 on these RNAs will inevitably impact the accuracy of the subsequent cleavage product sequence. This emphasizes the critical importance of studying the initial binding mode of Dcr-2 with esiRNA precursors. As the selected slm2 has a small closed loop at one end and a 2-nt overhang at its 3′ terminus, this type of structure is relatively stable. Unfortunately, in the initial binding state of Dcr-2/Loqs-PD with slm2, it is not possible to distinguish which end of slm2 binds to the Helicase domain due to the limited resolution of those regions in the cryo-EM map.

Our previous studies have shown that the correct cleavage of esiRNA precursors by Dcr-2/Loqs-PD involves Loqs-PD delivering the substrate RNA to Dcr-2's Helicase domain. Subsequently, ATP hydrolysis allows the substrate RNA to translocate through the Helicase domain, leading to cleavage. To investigate the end selection by the Dcr-2/Loqs-PD complex during processing, we designed two RNAs with variant ends: sl-closed, featuring a closed small loop at one end and a loose open structure at the opposite end and sl-open, with two loose open ends, similar to the wild-type pre-esiRNA (esi-2) (Fig. 5A). *In vitro* cleavage assays of the different RNA substrates indicated that, in comparison to Dcr-2 acting alone, the Dcr-2/Loqs-PD complex demonstrated notably higher cleavage activity on sl-closed (Supplementary Fig. S13A). In contrast, it exhibited negligible cleavage activity on sl-open (Supplementary Fig. S13B), suggesting that Dcr-2/Loqs-PD complex is proficient in processing RNAs featuring closed ends (Fig. 5B and C).

To further elucidate the loading capability of the Dcr-2/Loqs-PD complex for RNA substrates with flexible and open ends, we designed six additional distinct RNA duplexes derived from sl-open for *in vitro* cleavage assays (Fig. 6 and Supplementary Fig. S14). The presence of four unpaired nucleotides at the ends significantly reduced the catalytic efficiency of Dcr-2, particularly when these unpaired nucleotides were located at the 3′ terminus, which had a more pronounced negative impact on Dcr-2's cleavage efficiency compared to those at the 5′ terminus (Fig. 6B and C). Based on these experiments and analyses, we hypothesize that for wild-type esiRNA precursors, the Dcr-2/Loqs-PD complex initiates cleavage from the end that features the closed small loop.

Discussion

In *Drosophila*, esiRNA precursors processed by Dcr-2 in conjunction with Loqs-PD into esiRNAs play a pivotal role in silencing protein-coding genes and mobile elements. The esiRNA precursors are typically characterized by an extensive double-stranded region, with one end forming a compact loop and the opposite end exhibiting a more flexible open conformation comprised of 5′ and 3′ termini. Given the intricacy of this type of RNA structure, which poses a challenge for direct recognition by Dcr-2, the involvement of Loqs-PD becomes essential for facilitating more accurate recognition. Through our comprehensive cryo-EM structural and biochemical analysis, we have determined that the Dcr-2/Loqs-PD complex exhibits significant cleavage activity toward double-stranded RNAs with relatively rigid structures at one end, whereas it demonstrates minimal cleavage capability on ends characterized by open and loose conformations. These esiRNA pre-

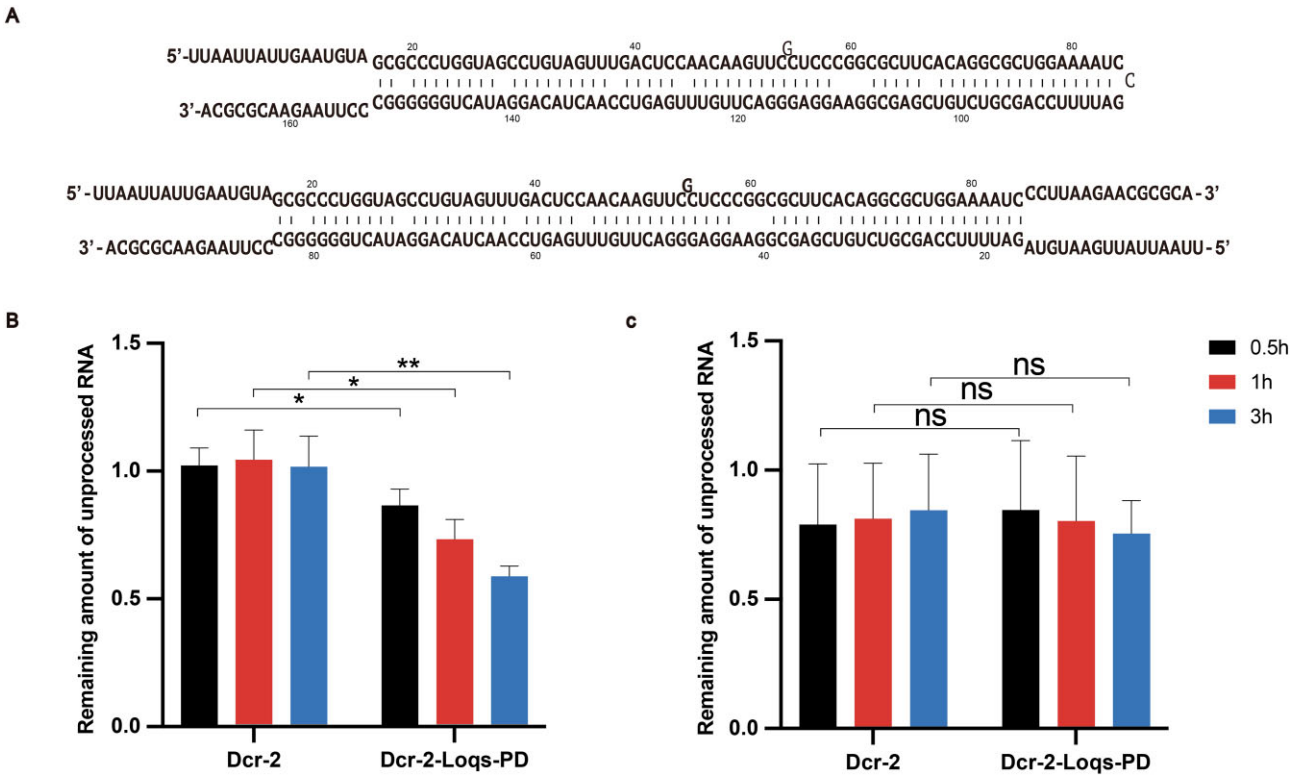

Figure 5. Ends selection of pre-esiRNA during processing by the Dcr-2/Loqs-PD complex. (**A**) Nucleotide sequences of the pre-esiRNAs, sl-closed (top), and sl-open (bottom) used in cleavage assay. (**B** and **C**) Quantification of cleavage assay of the Dcr-2 or Dcr-2/Loqs-PD with sl-closed (B) and sl-open (C), as performed in Supplementary Fig. S12. Error bars represent SD for three independent trials. *P*-value >.05, <.05, and <.01 are indicated by ns, *, and **, respectively.

cursors are preferentially loaded into the Helicase domain by Loqs-PD and subsequently translocated to the active site via ATP hydrolysis. Loqs-PD is crucial and indispensable in the precise processing of pre-esiRNA by Dcr-2. Moreover, mismatched nucleotides at the 3′-end can significantly decrease the likelihood of loading onto the Helicase domain. The presence of Loqs-PD preferentially recruits esiRNA precursors to the Helicase domain, whereas a loose open end of RNA substrates presents a challenge for binding to the Helicase domain, thereby impeding Dcr-2's ability to cleave such RNAs.

We observed distinct states formed by the Dcr-2 complex with slm1 and slm2, primarily arising from variations in the length of their respective stem regions. Given that Dcr-2/Loqs-PD can cleave both slm1 and slm2, it is theoretically possible that complexes formed with Dcr-2/Loqs-PD would exhibit both pre-dicing and dicing states for these substrates. However, we have not observed the dicing state for slm1 or the pre-dicing state for slm2. This is likely due to the difference in the length of the stable double-stranded regions of slm1 and slm2, which may result in only the pre-dicing state of slm1 and the dicing state of slm2 being stable when complexed with Dcr-2/Loqs-PD.

Previous work has shown that the cleavage of dsRNAs with blunt ends by Dcr-2 is ATP-dependent and generates cleavage products <21 nucleotides, indicating that the Platform/PAZ domains have rather weak binding ability or nonclassical binding modes with blunt-ended dsRNAs [55]. The Platform/PAZ domain may adopt a similar binding mode for those dsRNAs featuring a small closed loop structure at one end. Currently, despite the absence of structural evidence indicating that the Platform/PAZ domains can bind to the loop end of pre-esiRNA, the cleavage products resulting from slm2 processing at the closed loop end are discernible. It is noteworthy that in the case of slm2, cleavage results reveal the intriguing presence of ∼30 and ∼42 nt cleavage products mostly originating from the closed small loop end, which do not appear during the cleavage process starting from the 3′-end 2-nt overhang producing ∼21 and ∼60 nt cleavage products (red arrows) (Supplementary Fig. S3B). Therefore, this suggests that the inability of the closed small loop end to form a stable interaction with Dcr-2's PAZ domain may have hindered our ability to resolve the cryo-EM structure of this binding state during the cleavage process. However, slm1 does not exhibit obvious cleavage products from the loop end, which is likely due to the sequence and structural differences of slm1 and slm2. For slm2, we selected the natural loop end from esi-2, whereas slm1 was selected from the middle of esi-1. It is precisely because the loop end of slm2 retains its natural sequence and structural features that it is more susceptible to cleavage by Dcr-2/Loqs-PD at the loop end.

Although the Helicase domain exhibits a higher structural tolerance for substrate RNA, it still displays obvious preferences. As shown in our results, the end with a small closed loop or the shorter 3′ termini of pre-esiRNA are more recognizable by the Helicase domain than the loose open end. Additionally, previous studies have indicated that the Helicase domain can locally unwind bound dsRNAs [55]. Through the hydrolysis of ATP, the Helicase domain may promote the reorganization of certain unstable yet recognizable esiRNA precursors via a

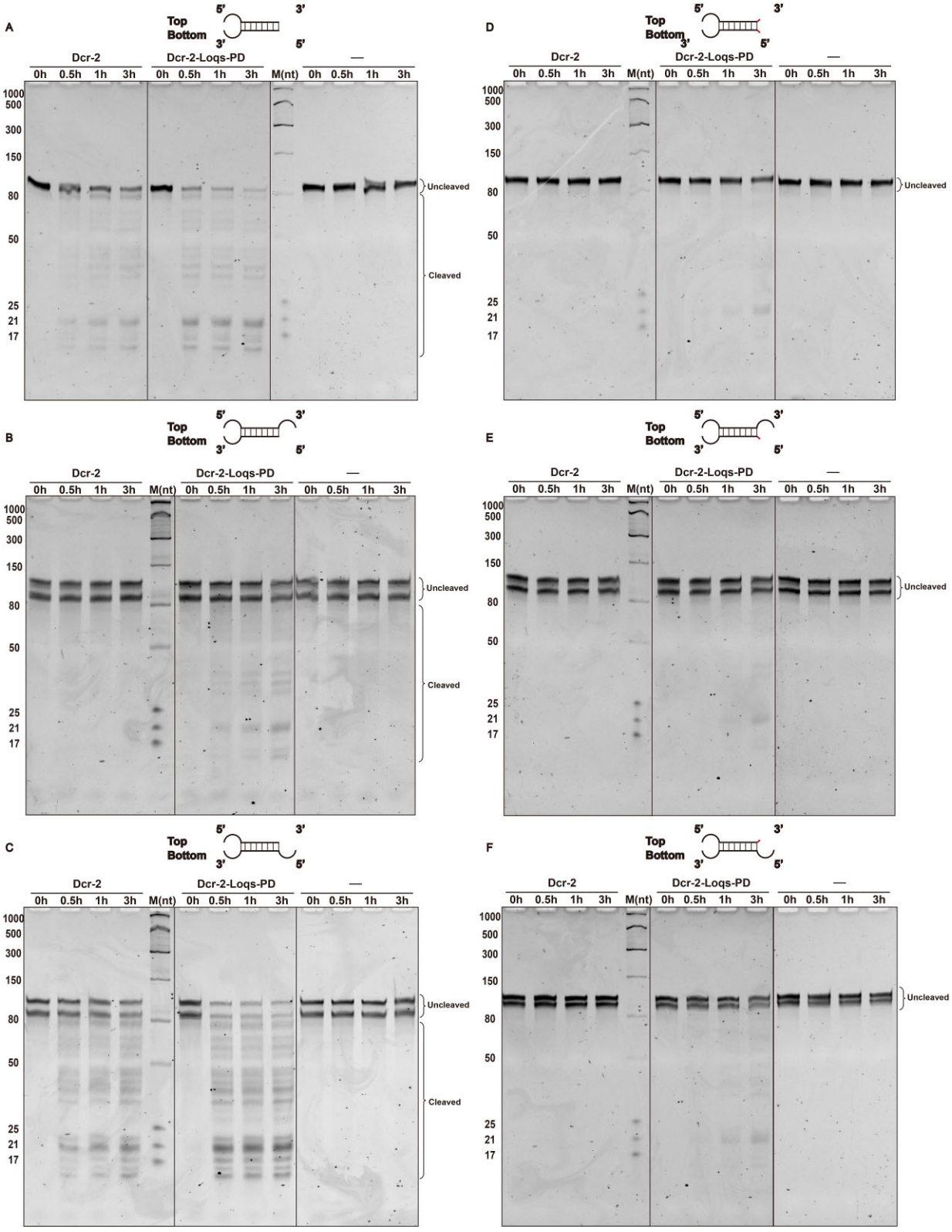

Figure 6. Pre-esiRNAs with different ends processing activities of Dcr-2 or Dcr-2/Loqs-PD. Cleavage assays of Dcr-2 or Dcr-2/Loqs-PD complex with pre-esiRNAs which have different length on the one end and the other end is same as sl-open, in the cleavage assay buffer (30°C). Pre-esiRNA with blunt terminal on the one end (**A**). Bottom ssRNA of pre-esiRNA without 5′ overhang (**B**). Top ssRNA of pre-esiRNA without 3′ overhang (**C**). Top ssRNA of pre-esiRNA with 3′-end 4-nt overhangs and bottom ssRNA of pre-esiRNA with 5′-end 4-nt overhangs (**D**). Bottom ssRNA of pre-esiRNA with 5′-end 4-nt overhangs (**E**). Top ssRNA of pre-esiRNA with 3′-end 4-nt overhangs (**F**). Four-nt overhangs originate from the corresponding longer top or bottom strands, respectively. Products were resolved on a 12% polyacrylamide denaturing gel. Schematic of the pre-esiRNAs is shown above the gel.

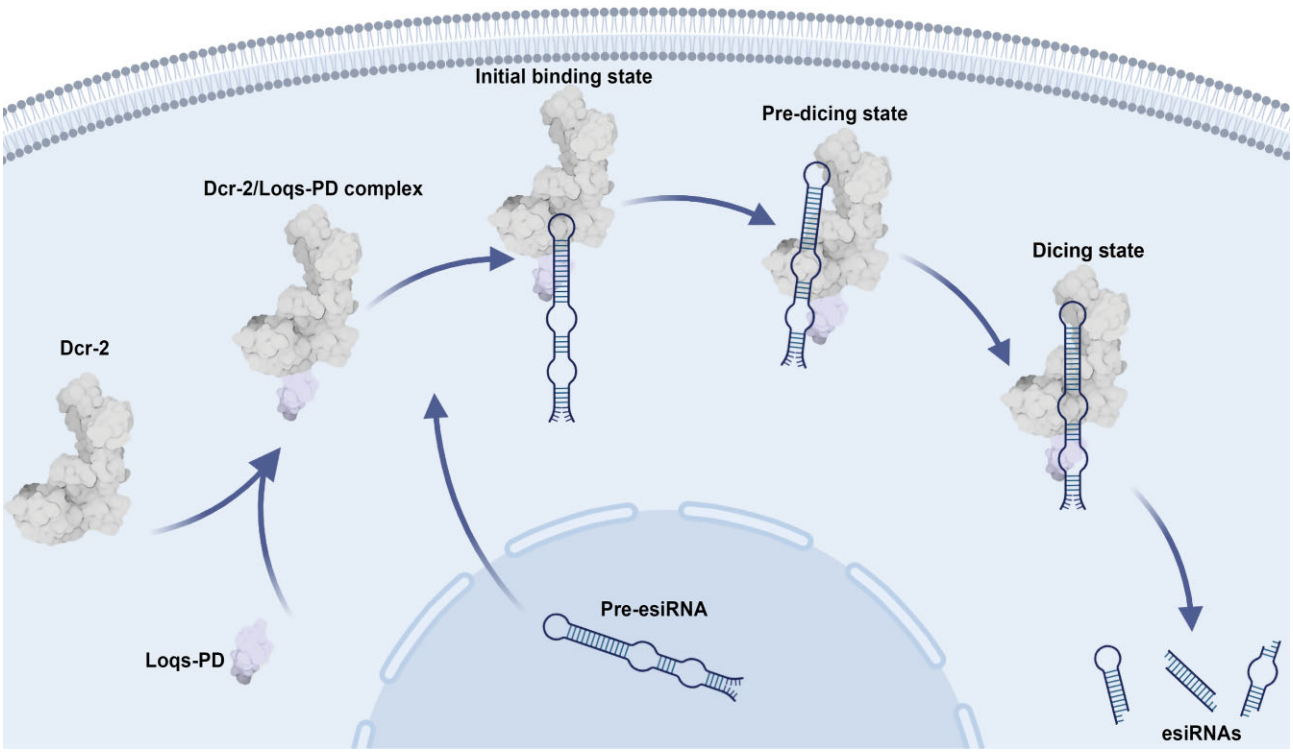

Figure 7. The model of the pre-esiRNA processing by the Dcr-2/Loqs-PD complex. With the assistance of the cofactor Loqs-PD, which is bound to the Helicase domain of Dcr-2, the small loop end of the pre-esiRNA, as opposed to its loose open end, is wrapped within the Helicase domain. Subsequently, upon the hydrolysis of ATP, the pre-esiRNA translocates upward through the Helicase domain and is conveyed to the Platform/PAZ domain. There, it engages in more extensive interactions with Dcr-2. Due to its proximity to the catalytic active site of Dcr-2, the cleavage process is facilitated, ultimately resulting in the production of a series of mature esiRNAs.

process of unwinding and refolding, thereby permitting their smooth passage through the domain and ensuring the precision of subsequent cleavage. After translocating through the Helicase domain and arriving at the Platform/PAZ domains, dsRNA of sufficient length undergoes cleavage. Intriguingly, during the dicing state, the conformations of various RNA substrates remain consistent.

Based on the above analysis, we delineate the dicing mechanism through which Dcr-2/Loqs-PD complex processes esiRNA precursors to generate esiRNA products (Fig. 7). Loqs-PD binds to the Helicase domain of Dcr-2 via its C-terminal region inducing Dcr-2 dimerization, and two tandem dsRBDs of Loqs-PD recruit the esiRNA precursor and load its end with a closed loop onto the Helicase domain of Dcr-2. Subsequently, the Helicase domain translocates the RNA substrate by ATP hydrolysis, and the Dcr-2 complex transitions to a monomeric state. Following the initial cleavage, the RNA acquires a 3′-end 2-nt overhang and 5′ monophosphate termini, which are efficiently identified by the Platform/PAZ domains. To ensure the correct and efficient cleavage of the bound substrate RNA, Dcr-2 maintains the dsRNA in a specific and fixed conformation during the cleavage process, which will guarantee the production of 21-nt cleavage products in a consecutive manner.

Acknowledgements

We thank Qinghua Liu from the National Institute of Biological Sciences, Beijing for the Dcr-2 plasmid. We thank Jianlin Lei and Fan Yang at Tsinghua University for assistance of data collection. We acknowledge the Tsinghua University Branch of the China National Center for Protein Sciences (Beijing) and Shuimu BioSciences Ltd. for providing the cryo-EM facility support and the computational facility support.

Author Contributions: H.-W.W., J.M., and J.W. conceived the study. N.C., J.W., T.D., S.S., J.M., and H.-W.W. designed experiments. N.C., T.D., B.F., S.S., and J.W. prepared the samples and performed the biochemical experiments and analyzed the data. N.C. and J.W. performed cryo-EM experiments, structure determination, and built the models. N.C., J.W., T.D., B.F., S.S, J.M., and H.-W.W. analyzed data. N.C., J.W., and H.-W.W. wrote the manuscript.

Supplementary data

Supplementary data is available at NAR online.

Funding

This research is supported by the National Natural Science Foundation of China (32130054 to H.-W.W. and 32471347 to J.M.) and Program of Shanghai Academic/Technology Research Leader (to J.M.). Funding to pay the Open Access publication charges for this article was provided by the National Natural Science Foundation of China (32130054).

Conflict of interest

None declared.

Data availability

Cryo-EM maps of the Dcr-2/Loqs-PD complexes with pre-esiRNA in initial binding states, pre-dicing states, and active-dicing states in this study with their associated atomic models have been deposited in the wwPDB OneDep System under EMD accession codes 39318, 39319, 39320, and PDB ID codes 8YIG, 8YIH, and 8YII, respectively. Cryo-EM maps of the Dcr-2 complexes with pre-esiRNA in pre-dicing state have been deposited in the wwPDB OneDep System under EMD accession code 39321. The PDB and EMDB codes are listed in Supplementary Table S1. For gel source images, see the Extended Data. All other data or materials can be obtained from the corresponding author upon request. Source data are provided with this paper.

References

1. Agrawal N, Dasaradhi PV, Mohmmed A *et al.* RNA interference: biology, mechanism, and applications. *Microbiol Mol Biol Rev* 2003;**67**:657–85. https://doi.org/10.1128/MMBR.67.4.657-685.2003
2. Cooper AM, Silver K, Zhang J *et al.* Molecular mechanisms influencing efficiency of RNA interference in insects. *Pest Manage Sci* 2019;**75**:18–28. https://doi.org/10.1002/ps.5126
3. Poterala A, Rzeszowska-Wolny J. The classification, structure and functioning of Ago proteins in eukaryotes. *Postepy Hig Med Dosw* 2016;**70**:1005–16. https://doi.org/10.5604/17322693.1220383
4. Daugaard I, Hansen TB. Biogenesis and function of ago-associated RNAs. *Trends Genet* 2017;**33**:208–19. https://doi.org/10.1016/j.tig.2017.01.003
5. Kutter C, Svoboda P. miRNA, siRNA, piRNA: knowns of the unknown. *RNA Biol* 2008;**5**:181–8. https://doi.org/10.4161/rna.7227
6. Grishok A. Biology and mechanisms of short RNAs in *Caenorhabditis elegans*. *Adv Genet* 2013;**83**:1–69. https://doi.org/10.1016/B978-0-12-407675-4.00001-8
7. Schwarz DS, Hutvagner G, Du T *et al.* Asymmetry in the assembly of the RNAi enzyme complex. *Cell* 2003;**115**:199–208. https://doi.org/10.1016/S0092-8674(03)00759-1
8. Lee YS, Nakahara K, Pham JW *et al.* Distinct roles for Drosophila Dicer-1 and Dicer-2 in the siRNA/miRNA silencing pathways. *Cell* 2004;**117**:69–81. https://doi.org/10.1016/S0092-8674(04)00261-2
9. Denli AM, Tops BB, Plasterk RH *et al.* Processing of primary microRNAs by the microprocessor complex. *Nature* 2004;**432**:231–5. https://doi.org/10.1038/nature03049
10. Jin W, Wang J, Liu CP *et al.* Structural basis for pri-miRNA recognition by Drosha. *Mol Cell* 2020;**78**:423–33. https://doi.org/10.1016/j.molcel.2020.02.024
11. Tsutsumi A, Kawamata T, Izumi N *et al.* Recognition of the pre-miRNA structure by Drosophila Dicer-1. *Nat Struct Mol Biol* 2011;**18**:1153–8. https://doi.org/10.1038/nsmb.2125
12. Forstemann K, Horwich MD, Wee L *et al.* Drosophila microRNAs are sorted into functionally distinct argonaute complexes after production by Dicer-1. *Cell* 2007;**130**:287–97. https://doi.org/10.1016/j.cell.2007.05.056
13. Lim MYT, Okamura K. Switches in dicer activity during oogenesis and early development. *Results Probl Cell Differ* 2017;**63**:325–51. https://doi.org/10.1007/978-3-319-60855-6_14
14. Iwasaki S, Sasaki HM, Sakaguchi Y *et al.* Defining fundamental steps in the assembly of the Drosophila RNAi enzyme complex. *Nature* 2015;**521**:533–6. https://doi.org/10.1038/nature14254
15. Forstemann K, Tomari Y, Du T *et al.* Normal microRNA maturation and germ-line stem cell maintenance requires Loquacious, a double-stranded RNA-binding domain protein. *PLoS Biol* 2005;**3**:e236. https://doi.org/10.1371/journal.pbio.0030236
16. Jiang F, Ye X, Liu X *et al.* Dicer-1 and R3D1-L catalyze microRNA maturation in Drosophila. *Genes Dev* 2005;**19**:1674–9. https://doi.org/10.1101/gad.1334005
17. Tabara H, Yigit E, Siomi H *et al.* The dsRNA binding protein RDE-4 interacts with RDE-1, DCR-1, and a DExH-box helicase to direct RNAi in *C. elegans*. *Cell* 2002;**109**:861–71. https://doi.org/10.1016/S0092-8674(02)00793-6
18. Partin AC, Zhang K, Jeong BC *et al.* Cryo-EM structures of Human drosha and DGCR8 in complex with primary microRNA. *Mol Cell* 2020;**78**:411–22. https://doi.org/10.1016/j.molcel.2020.02.016
19. Marques JT, Kim K, Wu PH *et al.* Loqs and R2D2 act sequentially in the siRNA pathway in Drosophila. *Nat Struct Mol Biol* 2010;**17**:24–30. https://doi.org/10.1038/nsmb.1735
20. Zhou R, Czech B, Brennecke J *et al.* Processing of drosophila endo-siRNAs depends on a specific Loquacious isoform. *RNA* 2009;**15**:1886–95. https://doi.org/10.1261/rna.1611309
21. Hartig JV, Esslinger S, Bottcher R *et al.* Endo-siRNAs depend on a new isoform of loquacious and target artificially introduced, high-copy sequences. *EMBO J* 2009;**28**:2932–44. https://doi.org/10.1038/emboj.2009.220
22. Fukunaga R, Han BW, Hung JH *et al.* Dicer partner proteins tune the length of mature miRNAs in flies and mammals. *Cell* 2012;**151**:533–46. https://doi.org/10.1016/j.cell.2012.09.027
23. Sinha NK, Trettin KD, Aruscavage PJ *et al.* Drosophila Dicer-2 cleavage is mediated by helicase- and dsRNA termini-dependent states that are modulated by Loquacious-PD. *Mol Cell* 2015;**58**:406–17. https://doi.org/10.1016/j.molcel.2015.03.012
24. Trettin KD, Sinha NK, Eckert DM *et al.* Loquacious-PD facilitates Drosophila Dicer-2 cleavage through interactions with the helicase domain and dsRNA. *Proc Natl Acad Sci USA* 2017;**114**:E7939–48. https://doi.org/10.1073/pnas.1707063114
25. Chung WJ, Okamura K, Martin R *et al.* Endogenous RNA interference provides a somatic defense against Drosophila transposons. *Curr Biol* 2008;**18**:795–802. https://doi.org/10.1016/j.cub.2008.05.006
26. Ghildiyal M, Seitz H, Horwich MD *et al.* Endogenous siRNAs derived from transposons and mRNAs in Drosophila somatic cells. *Science* 2008;**320**:1077–81. https://doi.org/10.1126/science.1157396
27. Pak J, Fire A. Distinct populations of primary and secondary effectors during RNAi in *C. elegans*. *Science* 2007;**315**:241–4. https://doi.org/10.1126/science.1132839
28. Ruby JG, Jan C, Player C *et al.* Large-scale sequencing reveals 21U-RNAs and additional microRNAs and endogenous siRNAs in *C. elegans*. *Cell* 2006;**127**:1193–207. https://doi.org/10.1016/j.cell.2006.10.040
29. Ghildiyal M, Zamore PD. Small silencing RNAs: an expanding universe. *Nat Rev Genet* 2009;**10**:94–108. https://doi.org/10.1038/nrg2504
30. Huisinga KL, Elgin SC. Small RNA-directed heterochromatin formation in the context of development: what flies might learn from fission yeast. *Biochim Biophys Acta* 2009;**1789**:3–16. https://doi.org/10.1016/j.bbagrm.2008.08.002
31. Verdel A, Vavasseur A, Le Gorrec M *et al.* Common themes in siRNA-mediated epigenetic silencing pathways. *Int J Dev Biol* 2009;**53**:245–57. https://doi.org/10.1387/ijdb.082691av
32. Tam OH, Aravin AA, Stein P *et al.* Pseudogene-derived small interfering RNAs regulate gene expression in mouse oocytes. *Nature* 2008;**453**:534–8. https://doi.org/10.1038/nature06904
33. Watanabe T, Totoki Y, Toyoda A *et al.* Endogenous siRNAs from naturally formed dsRNAs regulate transcripts in mouse oocytes. *Nature* 2008;**453**:539–43. https://doi.org/10.1038/nature06908
34. Flemr M, Malik R, Franke V *et al.* A retrotransposon-driven dicer isoform directs endogenous small interfering RNA production in mouse oocytes. *Cell* 2013;**155**:807–16. https://doi.org/10.1016/j.cell.2013.10.001
35. Chan WL, Yuo CY, Yang WK *et al.* Transcribed pseudogene psiPPM1K generates endogenous siRNA to suppress oncogenic

cell growth in hepatocellular carcinoma. *Nucleic Acids Res* 2013;**41**:3734–47. https://doi.org/10.1093/nar/gkt047
36. Okamura K, Lai EC. Endogenous small interfering RNAs in animals. *Nat Rev Mol Cell Biol* 2008;**9**:673–8. https://doi.org/10.1038/nrm2479
37. Miyoshi K, Miyoshi T, Hartig JV *et al.* Molecular mechanisms that funnel RNA precursors into endogenous small-interfering RNA and microRNA biogenesis pathways in Drosophila. *RNA* 2010;**16**:506–15. https://doi.org/10.1261/rna.1952110
38. Czech B, Malone CD, Zhou R *et al.* An endogenous small interfering RNA pathway in Drosophila. *Nature* 2008;**453**:798–802. https://doi.org/10.1038/nature07007
39. Okamura K, Chung WJ, Ruby JG *et al.* The Drosophila hairpin RNA pathway generates endogenous short interfering RNAs. *Nature* 2008;**453**:803–6. https://doi.org/10.1038/nature07015
40. Su S, Wang J, Deng T *et al.* Structural insights into dsRNA processing by Drosophila Dicer-2-loqs-PD. *Nature* 2022;**607**:399–406. https://doi.org/10.1038/s41586-022-04911-x
41. Liu N, Zheng L, Xu J *et al.* Reduced graphene oxide membrane as supporting film for high-resolution cryo-EM. *Biophys Rep* 2021;**7**:227–38.
42. Lei J, Frank J. Automated acquisition of cryo-electron micrographs for single particle reconstruction on an FEI Tecnai electron microscope. *J Struct Biol* 2005;**150**:69–80. https://doi.org/10.1016/j.jsb.2005.01.002
43. Zheng SQ, Palovcak E, Armache JP *et al.* MotionCor2: anisotropic correction of beam-induced motion for improved cryo-electron microscopy. *Nat Methods* 2017;**14**:331–2. https://doi.org/10.1038/nmeth.4193
44. Punjani A, Rubinstein JL, Fleet DJ *et al.* cryoSPARC: algorithms for rapid unsupervised cryo-EM structure determination. *Nat Methods* 2017;**14**:290–6. https://doi.org/10.1038/nmeth.4169
45. Rohou A, Grigorieff N. CTFFIND4: fast and accurate defocus estimation from electron micrographs. *J Struct Biol* 2015;**192**:216–21. https://doi.org/10.1016/j.jsb.2015.08.008
46. Goddard TD, Huang CC, Meng EC *et al.* UCSF ChimeraX: meeting modern challenges in visualization and analysis. *Protein Sci* 2018;**27**:14–25. https://doi.org/10.1002/pro.3235
47. Emsley P, Cowtan K. Coot: model-building tools for molecular graphics. *Acta Crystallogr D Biol Crystallogr* 2004;**60**:2126–32. https://doi.org/10.1107/S0907444904019158
48. Adams PD, Afonine PV, Bunkoczi G *et al.* PHENIX: a comprehensive Python-based system for macromolecular structure solution. *Acta Crystallogr D Biol Crystallogr* 2010;**66**:213–21. https://doi.org/10.1107/S0907444909052925
49. Court DL, Gan J, Liang YH *et al.* RNase III: genetics and function; structure and mechanism. *Annu Rev Genet* 2013;**47**:405–31. https://doi.org/10.1146/annurev-genet-110711-155618
50. Lee YY, Lee H, Kim H *et al.* Structure of the human DICER-pre-miRNA complex in a dicing state. *Nature* 2023;**615**:331–8. https://doi.org/10.1038/s41586-023-05723-3
51. Wang Q, Xue Y, Zhang L *et al.* Mechanism of siRNA production by a plant Dicer–RNA complex in dicing-competent conformation. *Science* 2021;**374**:1152–7. https://doi.org/10.1126/science.abl4546
52. Jouravleva K, Golovenko D, Demo G *et al.* Structural basis of microRNA biogenesis by Dicer-1 and its partner protein Loqs-PB. *Mol Cell* 2022;**82**:4049–63. https://doi.org/10.1016/j.molcel.2022.09.002
53. Tian B, Bevilacqua PC, Diegelman-Parente A *et al.* The double-stranded-RNA-binding motif: interference and much more. *Nat Rev Mol Cell Biol* 2004;**5**:1013–23. https://doi.org/10.1038/nrm1528
54. Masliah G, Barraud P, Allain FH. RNA recognition by double-stranded RNA binding domains: a matter of shape and sequence. *Cell Mol Life Sci* 2013;**70**:1875–95. https://doi.org/10.1007/s00018-012-1119-x
55. Sinha NK, Iwasa J, Shen PS *et al.* Dicer uses distinct modules for recognizing dsRNA termini. *Science* 2018;**359**:329–34. https://doi.org/10.1126/science.aaq0921

Received: October 30, 2024. **Revised:** January 21, 2025. **Editorial Decision:** January 31, 2025. **Accepted:** February 5, 2025